Accepted Manuscript

Studies on the Luminescence Properties of $CaZrO_3:Eu^{3+}$ Phosphors Prepared by the Solid State Reaction Method

Ishwar Prasad Sahu, D.P. Bisen, R.K. Tamrakar, K.V.R. Murthy, M. Mohapatra

PII: S2468-2179(16)30185-X

DOI: 10.1016/j.jsamd.2017.01.002

Reference: JSAMD 76

To appear in: *Journal of Science: Advanced Materials and Devices*

Received Date: 4 November 2016

Accepted Date: 17 January 2017

Please cite this article as: I.P. Sahu, D.P. Bisen, R.K. Tamrakar, K.V.R. Murthy, M. Mohapatra, Studies on the Luminescence Properties of $CaZrO_3:Eu^{3+}$ Phosphors Prepared by the Solid State Reaction Method, *Journal of Science: Advanced Materials and Devices* (2017), doi: 10.1016/j.jsamd.2017.01.002.

Studies on the Luminescence Properties of $CaZrO_3:Eu^{3+}$ Phosphors Prepared by the Solid State Reaction Method

[a]Ishwar Prasad Sahu*, [a]D.P. Bisen, [b]R.K. Tamrakar, [c]K.V.R. Murthy, [d]M. Mohapatra

[a]School of Studies in Physics & Astrophysics, Pt. Ravishankar Shukla University, Raipur (C.G.) Pin Code – 492010, India

[b]Department of Applied Physics, Bhilai Institute of Technology, Durg (C.G.) Pin Code - 491001, India

[c]Department of Applied Physics, The MS University of Baroda, Baroda, Gujarat, Pin Code – 390001, India

[d]Radiochemistry Division, Bhabha Atomic Research Centre, Mumbai (M.H.), Pin Code – 400085, India

Corresponding author Email ID – **ishwarprasad1986@gmail.com***

Studies on the Luminescence Properties of $CaZrO_3:Eu^{3+}$ Phosphors Prepared by the Solid State Reaction Method

[a]Ishwar Prasad Sahu*, [a]D.P. Bisen, [b]R.K. Tamrakar, [c]K.V.R. Murthy, [d]M. Mohapatra

[a]School of Studies in Physics & Astrophysics, Pt. Ravishankar Shukla University, Raipur (C.G.) Pin Code – 492010, India

[b]Department of Applied Physics, Bhilai Institute of Technology, Durg (C.G.) Pin Code - 491001, India

[c]Department of Applied Physics, The MS University of Baroda, Baroda, Gujarat, Pin Code – 390001, India

[d]Radiochemistry Division, Bhabha Atomic Research Centre, Mumbai (M.H.), Pin Code – 400085, India

Corresponding author Email ID – **ishwarprasad1986@gmail.com***

Abstract

Series of $CaZrO_3:xEu^{3+}$ (x = 1.0, 2.0, 3.0, 4.0 and 5.0 mole%) phosphors was successfully prepared by the solid state reaction method. The crystal structure of sintered phosphors was hexagonal phase with space group of Pm-3m. Near ultra-violet (NUV) excitation, emission spectra of $CaZrO_3:xEu^{3+}$ phosphors was composed of sharp line emission associated with the transitions from the excited states $^5D_0$ to the ground state $^7F_{j\ (j\ =\ 0,\ 1,\ 2,\ 3,\ 4)}$ of Eu^{3+}. The results indicated that the $CaZrO_3:xEu^{3+}$ might become an important orange-red phosphors candidate for white light emitting diodes (WLEDs) with near-UV LED chips. The peak of mechanoluminescence (ML) intensity increases linearly with increasing impact velocity of the moving piston, which suggests that sintered phosphors can be useful as a stress sensor.

Keywords: $CaZrO_3:Eu^{3+}$ phosphors; Decay; Color purity; WLEDs; Stress sensor.

1. Introduction

Today lighting and display industries are focused upon developing efficient high-intensity LED that produces white light. However, since white light is actually composed of many colors and LED produce monochromatic colors, this possesses a considerable challenge for LED technology [1, 2]. Presently, engineers have developed three systems for producing white light with LED; mixing red, green and blue (RGB) LED, UV LED with RGB phosphor coatings and blue LED with yellow phosphor coatings [3,4]. For example, the commonly used red phosphor $Y_2O_2S:Eu^{3+}$ shows lower efficiency compared with those of blue and green phosphors and instability due to release of a sulfide gas [5]. So it is necessary to find new red or orange-red phosphors, which should have a stable host, exhibit strong absorption and emission under 400nm excitation. Recently, considerable efforts have been devoted to the research of new orange-red materials used for white LEDs [6]. Quite a lot of luminescent materials activated by rare earth ions have been invented.

Thus, it is very essential to search a new orange-red light that can be used effectively to compensate the orange-red emission deficiency of the LED output light. For general lighting, photoluminescent materials including oxides, silicates, aluminates, alumino-borates, alumino-silicates, nitrides, borates etc., play very important for the potential applications in ultraviolet devices [7-12]. Oxides with perovskite structures are important materials with tunable compositions. This class of materials has attracted tremendous attention for their functional properties, such as ferro-electricity, piezo-electricity, pyro-electricity, non-linear dielectric behavior, as well as multi-ferroic property with wide applications in electronic industries [13, 14]. Among the perovskites calcium zirconate ($CaZrO_3$) is one of the material that has been extensively explored in the scientific community due its excellent electrical and thermo-

mechanical properties. Because of its inherent character to exhibit proton conductivity even at high temperatures, it is an ideal candidate to be used in sensors [15]. In recent years, rare earth doped $CaZrO_3$ materials have been widely investigated due to their significance to fundamental research and their high potential for application in optical materials [16]. According to Longo et al., the displacement of Zr or Ca atoms in disordered perovskite $CaZrO_3$ may induce some vacancy defects at the axial and planar oxygen sites of the [ZrO_6] octahedral [17]. It is well known that the vacancy defects may play important roles as not only carriers traps but also luminescence centers.

The optical properties include the thermoluminescence (TL) as well as mechanoluminescence (ML) of the materials. TL is the discharge of stored energy by thermal stimulation in the form of light [4]. ML is a type of luminescence caused by mechanical stimuli such as grinding, cutting, collision, striking and friction [12]. Up to now, some phosphors with high ML, such as red phosphors ($BaTiO_3$-$CaTiO_3$:Pr), green phosphors ($SrAl_2O_4$:Eu), yellow phosphors (ZnS:Mn) have been developed. However, these phosphors have low water resistance and lack variety in color, which have limited the application of ML sensors. It is well known ZrO_2 has a low thermal conductivity, high melting point, high thermal and mechanical resistance. It is used as an ideal medium for the fabrication of highly luminescent material due to its high refractive index, low phonon energy, high chemical and photochemical stability. ZrO_2 also plays an important role in the preparation of novel optical device materials [18].

In the present study, we have tested calcium zirconate ($CaZrO_3$) as a host lattice. Series of $CaZrO_3$:xEu^{3+} (x = 1.0, 2.0, 3.0. 4.0 and 5.0 mole%) phosphors were synthesized by the solid state reaction method. We report the structural characterization and optical properties of synthesized $CaZrO_3$:xEu^{3+} phosphors. The crystal structure and surface morphology were

analyzed by X-ray diffractometer (XRD) and field emission scanning electron microscopy (FESEM). Luminescence properties were also investigated on the basis of photoluminescence (PL), CIE; color purity; decay, thermoluminescence (TL); TL spectra; mechanoluminescence (ML); ML decay and ML spectrum techniques.

2. Experimental

2.1 Phosphors preparation

Series of europium doped calcium zirconate phosphors namely $CaZrO_3:xEu^{3+}$ (x = 1.0, 2.0, 3.0, 4.0 and 5.0 mole%) phosphors were synthesized by the conventional high temperature solid state reaction method. The raw materials were calcium carbonate [$CaCO_3$ (99.99%)], zirconium oxide [ZrO_2 (99.99%)] and europium oxide [Eu_2O_3 (99.99%)], all of analytical grade were employed in this experiment. Boric acid [H_3BO_3 (99.99%)] was added as a flux. Initially, the raw materials were weighed according to the nominal compositions of $CaZrO_3:xEu^{3+}$ phosphors, then the powders were mixed and milled thoroughly for 3 hours using mortar and pestle. The chemical reaction used for stoichiometry calculation was:

$$2CaCO_3 + 2ZrO_2 + 2Eu_2O_3 \xrightarrow{1300^oC} 2CaZrO_3:Eu^{3+} + 2CO_2 + 3O_2 \uparrow$$

The ground samples were placed in an alumina crucible and subsequently fired at 1300°C for 4 hours in an air. At last the nominal compounds were obtained after the cooling down of programmable furnace and products were finally grounded into powder for characterizing the phosphors.

2.2 Measurement techniques

The powder XRD pattern of the prepared $CaZrO_3:xEu^{3+}$ phosphors have been obtained from the Bruker D8 advanced X-ray powder diffractometer using CuKα (1.54060 Å) radiation

and the data were collected over the 2θ range 10-80^{o}. The surface morphological images of optimum concentration [$CaZrO_3:Eu^{3+}$ (3.0%)] phosphor was collected by the FESEM. The samples were coated with a thin layer of gold (Au) and then the surface morphology of prepared phosphor was observed by the FESEM; Bruker, operated at the acceleration voltage of 18 kV. TL glow curves were recorded with the help of TLD reader 1009I by Nucleonix (Hyderabad, India Pvt. Ltd.). Every time of the TL measurement, quantity of the powder samples were kept fixed (8 mg). Excitation and emission spectra of synthesized phosphors were recorded on a spectrofluorophotometer, Shimadzu (RF 5301-PC) using the Xenon lamp (150 W) as the excitation source when measuring. Color chromaticity coordinates were obtained according to Commission International de I'Eclairage (CIE) 1931. Decay curves were obtained using a time resolved fluorescence spectroscopy (TRFS) from Horiba Jobin Yvon IBH to measure the fluorescence lifetimes of the prepared $CaZrO_3:Eu^{3+}$ (3.0%) phosphor (using pulsed lasers as excitation source). The ML measurement was observed by the homemade lab system comprising of an RCA-931A photomultiplier tube (PMT). The ML glow curve can be plotted with the help of SM-340 application software installed in a computer attached with the storage oscilloscope (19). All measurements were carried out at the room temperature.

3. Results and discussion

3.1 XRD analysis

In order to determine the crystal structure of synthesized phosphors, powder XRD analysis has been carried out. Typical XRD patterns of $CaZrO_3$ and $CaZrO_3:xEu^{3+}$ (x = 1.0, 2.0, 3.0, 4.0 and 5.0 mole%) phosphors with the standard XRD pattern was shown in Fig. 1 (a). The position and intensity of diffraction peaks of prepared $CaZrO_3$ and $CaZrO_3:xEu^{3+}$ phosphors were matched and found to be consistent with the Joint Committee of Powder Diffraction

Standard data (JCPDS) file (JCPDS:20-0254) [20], indicating that the doping of Eu^{3+} ions does not cause any significant change in the host structure. A comparison of the data with the standard JCPDS file reveals that the diffraction peaks of the $CaZrO_3:xEu^{3+}$ phosphors match with those of the standard hexagonal phase with the space group of Pm-3m (221). The atomic parameters of $CaZrO_3$ phosphor were shown in Table 1.

Fig. 1 (a) XRD patterns of $CaZrO_3$ and $CaZrO_3:Eu^{3+}$ phosphors with different Eu^{3+} concentration (b) Crystal structure and cation polyhedral arrangements of polymorph $CaZrO_3$ phosphor (c) FESEM image of $CaZrO_3:Eu^{3+}$ (3.0%) phosphor

Table 1 Atomic parameters of $CaZrO_3$ phosphor

Based on Pauli theory and the effective, ionic radius of cations, it was deduced that Eu^{3+} should be expected to occupy the Ca^{2+} sites, preferably, since the ionic radius of Eu^{3+} (1.07 Å) is close to the Ca^{2+} (1.12 Å) ions compared with the ionic radii of Zr^{4+} (0.57 Å). Fig. 1 (b) shows crystal structures and the coordination polyhedral of Eu^{3+} (or Ca^{2+}) ions surrounded by O^{2-} ions for $CaZrO_3:xEu^{3+}$ phosphors. The lattice parameters of the optimum $CaZrO_3:xEu^{3+}$ (3.0%) phosphor was calculated using Celref V3 software. The refined values of hexagonal europium doped calcium zirconate were found as; a = b = c = 4.0191 Å, $\alpha = \beta = \gamma = 90^{o}$ and cell volume (V) = 64.92 $(Å)^3$, Z = 1, is nearly same [a = b = c = 4.0200 Å, $\alpha = \beta = \gamma = 90^{o}$ and cell volume (V) = 64.96 $(Å)^3$, Z = 1], with the standard lattice parameters which again signifies the proper preparation of the discussed $CaZrO_3:xEu^{3+}$ (3.0%) phosphor.

FESEM studies were carried out to obtain information about surface morphology, grain size and shape of the synthesized optimum $CaZrO_3:xEu^{3+}$ (3.0%) phosphor. The morphologies of prepared $CaZrO_3:xEu^{3+}$ (3.0%) phosphor was also observed by means of FESEM with different magnification in Fig. 1 (c). The micrographs demonstrate that the sample sizes are varying from

a few microns to several tens of microns and form a large secondary particle. The surface of the discussed phosphor has shown irregular shape which means the distribution of the particle sizes was not homogeneous. From the FESEM image, it can be observed that the prepared phosphor consists of particles with different size distribution. FESEM examination showed that the particle shape and size of the solid state reaction depended significantly on the synthesis procedure. It is ascribed to that the solid state reaction used in this study requires a high temperature, which induces sintering and aggregation of particles, and it is an advantage for perfect crystal formation.

3.2 Photoluminescence (PL)

In order to facilitate the analysis of the optical properties of $CaZrO_3:xEu^{3+}$ (x = 1.0, 2.0, 3.0, 4.0 and 5.0 mole%) phosphors and their luminescent properties under NUV excitation were investigated in detail. The excitation and emission spectrum of $CaZrO_3:xEu^{3+}$ phosphors were monitored at 593 nm and 395 nm were displayed in Fig. 2. The excitation spectrum of $CaZrO_3:xEu^{3+}$ phosphors exhibit a broad band in the UV region centered at about 249 nm, and several sharp lines lies in the range of 300 to 500 nm. It can be seen from Fig. 2, the excitation spectrum is composed of two major parts: (1) the broadband between 220 and 300 nm, the broad absorption band is called charge transfer (CT) state band due to the europium-oxygen interactions, which is caused by an electron transfer from an oxygen 2p orbital to an empty 4f shell of europium and the strongest excitation peak is at about 249 nm [21]. (2) A series of sharp lines between 300 to 500 nm, ascribed to the f-f transition of Eu^{3+}. The strongest sharp peak is located at 395 nm corresponding to $^7F_0 \rightarrow {}^5L_6$ transition of Eu^{3+} ions. Other weak excitation peaks were located at 320, 363, 383, 417 and 466 nm are related to the intra-configurational 4f–4f transitions of Eu^{3+} ions in the host lattices, which can be assigned to $^7F_0 \rightarrow {}^5H_6$, $^7F_0 \rightarrow {}^5D_4$, $^7F_0$

$\rightarrow$ $^5G_4$, $^7F_0 \rightarrow {}^5D_3$ and $^7F_0 \rightarrow {}^5D_2$ transitions, respectively. The prepared $CaZrO_3:xEu^{3+}$ phosphors can be excited by near UV (NUV) at about 395 nm effectively. So, it can match well with UV and NUV-LED, showing a great potential for practical applications [22].

Fig. 2 Excitation and emission spectra of $CaZrO_3:xEu^{3+}$ phosphors with different Eu^{3+} concentration

From the excitation and emission spectra of $CaZrO_3:Eu^{3+}$, the characteristics of this excitation spectrum showed some remarkable differences from that reported by Dubey et al. [23], which reported that the intensity of f–f absorption transition of Eu^{3+} at 393 nm is much lower than that the CT absorption band (CTB absorption in $CaZrO_3:Eu^{3+}$ is dominated). However, our experiment data indicated that the CTB absorption in $CaZrO_3:xEu^{3+}$ is not dominated. As a result, it can match well with the radiation of NUV InGaN-based LED chip.

Fig. 2 shows the emission spectra of $CaZrO_3:xEu^{3+}$ phosphors with different concentration of (x = 1.0, 2.0, 3.0, 4.0 and 5.0 mole%) was recorded in the range of 450 to 750 nm. Under the 395 nm excitation, emission spectrum of obtained phosphors was composed of a series of sharp emission lines, corresponding to transitions from the excited states $^5D_0$ to the ground state $^7F_{j\ (j = 0, 1, 2, 3, 4)}$ in the $4f^6$ configuration of Eu^{3+} ions, among which the main emission line is located at around 593 nm **.** The orange emission at about 593 nm belongs to the magnetic dipole $^5D_0 \rightarrow {}^7F_1$ transition of Eu^{3+} ions, and the transition hardly varies with the crystal field strength. The red emission at 615 nm ascribes to the electric dipole $^5D_0 \rightarrow {}^7F_2$ transition of Eu^{3+}, which is very sensitive to the local environment around the Eu^{3+}, and depends on the symmetry of the crystal field [23]. It is found that the 593 and 615 nm emissions are the two strongest peaks, indicating that there are two Ca^{2+} sites in the $CaZrO_3$ lattice. One site, Ca (I), is inversion symmetry and the other site, Ca (II), is non-inversion symmetry. When Eu^{3+} ions were doped in

$CaZrO_3$ host; they occupied two different sites of Ca (I) and Ca (II). Other three emission peaks were located at 580, 652 and 703 nm; are relatively weak, corresponding to the $^5D_0 \rightarrow ^7F_{0;}$ $^5D_0 \rightarrow ^7F_3$ and $^5D_0 \rightarrow ^7F_4$ typical transitions of Eu^{3+} ions respectively. For the $CaZrO_3:xEu^{3+}$ phosphors, prepared in our experiment, the strongest orange emission peak is located at 593 nm will be dominated. It can be presumed that Eu^{3+} ions mainly occupy with inversion symmetric center in the host lattice [24].

To investigate the concentration dependent luminescent property of Eu^{3+} ions doped $CaZrO_3$ host, a series of $CaZrO_3:xEu^{3+}$ (3.0%) phosphors were synthesized and the luminescent properties were measured are shown in Fig. 2. It can be seen that all the emission spectra are similar regardless of Eu^{3+} contents. In $CaZrO_3$ host, the Eu^{3+} impurity concentration was increased in the range from 1.0 mole% to 3.0 mole% and the maximum emission intensity was observed at 3.0 mole%. Eu^{3+} concentration (x) dependence of the emission intensities is shown in the Fig. 2. The concentration quenching was observed for higher doping concentration of Eu^{3+}. If there is an increase in concentration of the lanthanide ions in a given material it should be accompanied by an increase in the emitted light intensity, but it has been established that such behavior occurs up to a certain critical concentration. Above this critical concentration the luminescence intensity starts to decrease. This process is known as concentration quenching of the luminescence [25].

The concentration quenching is due to energy transfer from one activator (donor) to another until the energy sink (acceptor) in the lattice is reached. Hence, the energy transfer will strongly depend on the distance (R_c) between the Eu^{3+} ions, which can be obtained using the following equation (1) [26].

$$R_c \approx 2\left[\frac{3V}{4\pi X_c Z}\right]^{\frac{1}{3}} \quad (1)$$

Where X_c is the critical concentration, Z is the number of cation sites in the $CaZrO_3$ unit cell [Z = 1 in $CaZrO_3$], and V is the volume of the unit cell (V = 64.92 (Å)^3 in this case). The critical concentration is estimated to be about x = 3.0 mole%, where the measured emission intensity begins to decrease. The critical distance (R_c) between the donor and acceptor can be calculated from the critical concentration, for which the nonradiative transfer rate equals the internal decay rate (radiative rate). Blasse [27, 28] assumed that, for the critical concentration, the average shortest distance between the nearest activator ions is equal to the critical distance. By taking the experimental and analytic values of V, Z and X_c [64.92 (Å)^3, 1, 3.0 mole%, respectively], the critical distance R_c is estimated by Equation (1) is equal to 16.05 Å in this host. The value of R_c is greater than 5 Å for the rare earth ions indicating that the multipole–multipole interaction is dominant and is the major cause of concentration quenching of Eu^{3+} in the phosphors.

3.3 CIE Chromaticity Coordinate

The chromaticity diagram is a tool to specify how the human eye will experience light with a given spectrum. The luminescence color of the samples were excited under 395 nm has been characterized by the CIE (Commission International de I'Eclairage) 1931 chromaticity diagram. The emission spectrum of the $CaZrO_3:Eu^{3+}$ (3.0%) phosphor was converted to the CIE 1931 chromaticity using the photo-luminescent data and the interactive CIE software (CIE coordinates calculator) [29] diagram as shown in Fig. 3.

Fig. 3 CIE chromaticity diagram of $CaZrO_3:Eu^{3+}$ (3.0%) phosphor

Every natural color can be identified by (x, y) coordinates that are disposed inside the 'chromatic shoe' representing the saturated colors. Luminescence colors of $CaZrO_3:Eu^{3+}$ (3.0%) phosphor is placed in (x = 0.6092, y = 0.3836), which is represented by the circle symbol "o". The chromatic co-ordinates of the luminescence of this phosphor are measured and reached near to orange-red luminescence. The other prepared $CaZrO_3:xEu^{3+}$ (x = 1.0, 2.0, 4.0 and 5.0%) phosphors were also placed in (x = 0.6017, y = 0.3883); (x = 0.6065, y = 0.3856); (x = 0.6076, y = 0.3844) and (x = 0.5927, y = 0.3945) corners respectively [Inset Fig. 3]. The chromatic co-ordinates of the luminescence of all the sintered phosphors were measured and reached to near orange-red emission.

The chromaticity diagram of the CIE indicates the coordinates are highly useful in determining the exact emission color and color purity of a sample. Because the color purity is considered as one of the important factors for evaluating the performance of phosphors, the color purity of samples has been calculated by the following equation (2) [27]:

$$\text{Color purity} = \frac{\sqrt{(x-x_i)^2+(y-y_i)^2}}{\sqrt{(x_d-x_i)^2+(y_d-y_i)^2}} \cdot 100\% \qquad (2)$$

Where (x, y) and (x_i, y_i) are the color coordinates of the light source and the CIE equal-energy illuminant respectively; (x_d, y_d) is the chromaticity coordinate corresponding to the dominant wavelength of light source. For $CaZrO_3:xEu^{3+}$ (x = 1.0, 2.0, 3.0, 4.0 and 5.0%) phosphors, and the coordinates of (x, y) are (x = 0.6017, y = 0.3883); (x = 0.6065, y = 0.3856); (x = 0.6092, y = 0.3836); (x = 0.6076, y = 0.3844) and (x = 0.5927, y = 0.3945) respectively; the coordinates of (x_i, y_i) are (0.3333, 0.3333); (x_d, y_d) is (x = 0.6069, y = 0.3908); (x = 0.6092, y = 0.3891); (x = 0.6099, y = 0.3842); (x = 0.6094, y = 0.3853) and (x = 0.5959, y = 0.3967)

corresponding to the dominant wavelength 593 nm. Based on these coordinate values and equation (2), we finally get the color purity of $CaZrO_3:xEu^{3+}$ (x = 1.0, 2.0, 3.0, 4.0 and 5.0%) phosphors as 97.99%, 98.81%, 99.71%, 99.31% and 98.65% respectively. It is worthwhile to mention that the CIE chromaticity coordinate of $CaZrO_3:Eu^{3+}$ (3.0%) phosphors are very close to those corresponding dominant wavelength points, and that almost pure white color purity phosphors have been obtained in our work.

3.4 Decay

Fig. 4 shows typical decay curves of $CaZrO_3:Eu^{3+}$ (3.0%) phosphor. The initial intensity of the sintered $CaZrO_3:Eu^{3+}$ (3.0%) phosphor was high. The decay times of phosphor can be calculated by a curve fitting technique, and decay curves fitted by the sum of two exponential components have different decay times.

$$I = A_1 \exp(-t/\tau_1) + A_2 \exp(-t/\tau_2) \quad (3)$$

Where, I is phosphorescence intensity, A_1, A_2 are constants, t is time, τ_1 and τ_2 are decay times (in millisecond) for the exponential components. Decay curves are successfully fitted by the equation (3) and the fitting curve result are shown in the inset of Fig. 4 with the standard error. The results indicated that the prepared $CaZrO_3:Eu^{3+}$ (3.0%) phosphor shows a rapid decay and the subsequent slow decaying process [30].

Fig. 4 Decay curves of $CaZrO_3:Eu^{3+}$ (3.0%) phosphor

As it was reported before, when Eu^{3+} ions were doped into $CaZrO_3$, they would substitute the Ca^{2+} ions. To keep electroneutrality of the compound, two Eu^{3+} ions would substitute three Ca^{2+} ions. The process can be expressed as

$$2Eu^{3+} + Ca^{2+} \longrightarrow 2[Eu_{Ca}]^* + [V_{Ca}]'' \quad (4)$$

Each substitution of two Eu^{3+} ions would create two positive defects of $[Eu_{Ca}]^*$ capturing electrons and one negative vacancy of $[V_{Ca}]''$. These defects act as trapping centers for charge carriers. Then the vacancy $[V_{Ca}]''$ would act as a donor of electrons while the two $[Eu_{Ca}]^*$ defects become acceptors of electrons. By thermal stimulation, electrons of the $[V_{Ca}]''$ vacancies would then transfer to the Eu^{3+} sites. The results indicate that the depth of the trap is too shallow leading to a quick escape of charge carriers from the traps resulting in a fast recombination rate in millisecond (ms) [31, 32].

3.5 Thermoluminescence (TL)

In order to study the trap states of the prepared $CaZrO_3:xEu^{3+}$ (x = 1.0, 2.0, 3.0, 4.0 and 5.0 mole%) phosphors, TL glow curves were measured and shown in Fig. 5 (a). The synthesized phosphors were first irradiated for 5 min using 365 nm UV source, then the radiation source was removed and the irradiated samples were heated at a linear heating rate of $5^oC/s$, from room temperatures to 250^oC. Initially, TL intensity increases with temperature, attains a peak value for a particular temperature and then it decreases with further increase in temperature. A single glow peak of $CaZrO_3:xEu^{3+}$phosphors were obtained at 113.31^oC. The single isolated peak due to the formation of only one type of luminescence center which is created due to the UV irradiation. It is suggested that the recombination center associated with the glow at the temperature interval arises from the presence of liberated pairs, which are probably the results from the thermal release of electron/holes from different kinds of traps and recombine at the color centers. It is also known that the doping of the rare earth ions increases the lattice defects which have existed already in the host. The position of the TL peaks keeps almost constant in the concentration range studied. It is observed that the intensity of this glow peak is found to increase with the increase of Eu^{3+} concentration up to x = 3.0% and then decreases for higher concentration i.e.,

for x = 3.0%. The TL intensity decrease due to concentration quenching of Eu^{3+} ions. The TL signal steadily increased after incorporation of Eu^{3+} ions, which are well known as efficient activators in many materials. In the present study it is observed that the glow curve shapes of europium doped samples are similar, indicating that there are interactions of intrinsic defects and doped impurities [33]. The different TL parameters calculations are listed in Table 2.

Fig. 5 (a) Comparative TL glow curve of $CaZrO_3$:xEu^{3+} phosphors with different Eu^{3+} concentration at 5 minute UV irradiation

Fig. 5 (b) shows the effect of UV dose on TL intensity for 3.0 mole% Eu^{3+} doped $CaZrO_3$ phosphor. The TL glow curve peak occurred at 113.31^{o}C and these peak positions remains constant with UV irradiation time. From the TL glow curve, it is seen that, initially TL intensity increase with increasing UV irradiation time. TL intensity are maximum for 20 min of UV exposure, after that they start to decrease. It is predicted that with the increasing UV irradiation time, greater number of charge carriers are released which increases the trap density results in increase of TL intensity (density of charge carrier may have been increasing), but after a specific exposure (20 min) traps starts to destroy results in decrease in TL intensity. The decreasing of charge carriers density is may be a reason for the low TL intensity at higher irradiation time (25 minute). Further, there was no appreciable shift was observed in the glow peak position for higher irradiation doses [34].

Fig. 5 (b) Comparative TL glow curve of $CaZrO_3$:Eu^{3+} (3.0%) phosphor for different UV irradiation time

3.5.1 Determination of kinetic parameters

Thermally stimulated luminescence is one of the most studied subjects in the field of condensed matter physics and a complete description of the thermoluminescent characteristics of a TL material requires obtaining these parameters. There are various methods for evaluating the trapping parameters [i.e. activation energy (E), order of kinetics (b) and frequency factor (s),] from TL glow curves [35]. TL parameters of prepared phosphors were calculated using the peak shape method. The relationship between the frequency factor's' and the activation energy 'E' is given by the equation (5)

$$\frac{\beta E}{kT_m^2} = s\left[1+(b-1)\frac{2kT_m}{E}\right]\exp(E/KT_m) \tag{5}$$

Where, k is Boltzmann constant, E is activation energy, b is order of kinetics, T_m is temperature of peak position, and β is the heating rate. In the present work β = 5^{o}Cs^{-1}. Trap depth for second order kinetics is calculated using the equation (6)

$$E = 2kT_m\left(1.76\frac{T_m}{\omega}-1\right) \tag{6}$$

Where, ω is the total half width intensity $\omega = \tau+\delta$, τ is the half width at the low temperature side of the peak ($\tau = T_m-T_1$); δ is the half width towards the fall-off side of the glow peak ($\delta = T_2-T_m$), and T_m is the peak temperature at the maximum. Chen provides a method which can identify the kinetics order for a model of one trap according to the shape of the TL band. The method involves the parameter μ_g ($\mu_g = \delta/\omega$). The shape factor (μ_g) is to differentiate between first and second order TL glow peak. (μ_g) = 0.39 - 0.42 for the first order kinetics, (μ_g) = 0.42 – 0.48 for the non-first order kinetics (mixed order) and (μ_g) = 0.49 - 0.52 for the second order kinetics [36]. In our case, for the $CaZrO_3$:xEu^{3+} phosphors; shape factor (μ_g) is lying

between 0.47 to 0.50, which indicates that it is a case of non-first order kinetics, approaching towards second order, responsible for deeper trap depth.

Table 2 Activation Energy (E), Shape factor (μ_g) and Frequency Factor (s) for 5 minute UV irradiated $CaZrO_3:xEu^{3+}$ phosphors for different Eu^{3+} concentration

The TL kinetic parameters of $CaZrO_3:Eu^{3+}$ (3.0%) phosphor was also calculated by the peak shape method and details are given in Table 3. In our case, the value of shape factor (μ_g) of $CaZrO_3:Eu^{3+}$ (3.0%) phosphor was lies between 0.48 to 0.50, which indicates that it is a case of non-first order kinetics, approaching towards second order, responsible for deeper trap depth. When the deep trap was created, the probability of re-trapping is high. It should also be noted that if the traps are too deep, it is not possible for UV excitation source to overcome the energy of a very deep trap at room temperature [37].

Table 3 Activation Energy (E), Shape factor (μ_g) and Frequency Factor (s) for $CaZrO_3:Eu^{3+}$ (3.0%) phosphor for different UV irradiation time

3.6 Mechanoluminecsnce (ML)

In the present ML studies, an impulsive deformation technique has been used [38]. When a moving piston (400gm load) was applied onto the phosphor, initially the ML intensity increases with time, attains a peak value and then decreases with time. Such a curve between the ML intensity and the deformation time of phosphors is known as the ML glow curve [39] Fig. 6 (a) shows that the comparative ML glows curve of $CaZrO_3:xEu^{3+}$ phosphors for fixed height (h = 50 cm). The phosphor was fracture via dropping a load [moving piston] of particular mass and cylindrical shape on the $CaZrO_3:xEu^{3+}$ phosphors. When the moving piston is dropped onto the prepared phosphors at 50 cm height, a great number of physical processes may occur within very short time intervals, which may excite or stimulate the process of photon emission and light is

emitted. The photon emission time is nearly 2 ms, when prepared $CaZrO_3:xEu^{3+}$ phosphors fractures. In these ML measurements, maximum ML intensity has been observed for $CaZrO_3:Eu^{3+}$ (3.0%) phosphor. The prepared phosphor was fracture without any pre-irradiation such as X-ray, β- rays, γ-rays, UV, etc.

Fig. 6 (a) Comparative ML glow curve of $CaZrO_3:xEu^{3+}$ phosphors

Fig 6 (b) shows that the characteristics ML glow curve between ML intensity versus time for $CaZrO_3:Eu^{3+}$ (3.0%) phosphor at different heights (h = 10, 20, 30, 40, 50 cm). The velocity of the moving piston, holding the impact mass, could be changed, by changing the height through which it was dropped. In these ML measurements, maximum ML intensity has been obtained for the 50 cm dropping height and ML intensity increases linearly with the increases the falling height of the moving piston [inset Fig. 6 (b)]. The ML intensity of $CaZrO_3:xEu^{3+}$ (3.0%) phosphor increases linearly with increasing the mechanical stress

Fig. 6 (b) ML intensity versus time curve of $CaZrO_3:Eu^{3+}$ (3.0%) phosphor

(Inset - ML intensity versus impact velocity curve of $CaZrO_3:Eu^{3+}$ (3.0%) phosphor)

The relationship between semi-log plot of ML intensity versus $(t-t_m)$ for $CaZrO_3:Eu^{3+}$ (3.0%) phosphor is shown in Fig. 7, and the lines were fitted using the following equation (7) with Origin 8.0

$$\tau = \frac{1}{slope\ of\ straight\ line} \tag{7}$$

Curve fitting results show that the decay constant (τ) varies from 0.89 to 1.04 ms. The ML decay constant value is the maximum for the low impact velocities (Table 4). The Decay rates of the exponentially decaying period of the ML curves did not change significantly with

impact velocity. In order to further clarify of the ML decay mechanism in $CaZrO_3:Eu^{3+}$ (3.0%) phosphor, more experimental and theoretical studies are needed.

Fig. 7 Semi-log plot of ML intensity versus ($t-t_m$) for $CaZrO_3:Eu^{3+}$ (3.0%) phosphor

Table 4 Calculation of ML decay constant for $CaZrO_3:Eu^{3+}$ (3.0%) phosphor

When a mechanical stress, such as compress, friction, and striking, and so on, were applied onto the sintered $CaZrO_3:xEu^{3+}$ phosphors, a local piezoelectric field can be produced. Therefore, in such phosphors the ML excitation may be caused by the local piezoelectric field near the impurities and defects in the crystals [40]. During the impact on the material, one of its newly created surfaces gets positively charged and other surface of the crack gets negatively charged. Thus, an intense electric field in the order of 10^6 - 10^7 Volt/cm is produced [44]. Under such order of electric field, the ejected electrons from the negatively charged surface may be accelerated and subsequently their impact on the positively charged surfaces may excite the luminescence center. Subsequently, the de-excitation of excited Eu^{3+} ions may give rise to the light emission due to the transition from an excited state to ground state respectively. As the height of the piston increases the area of newly created surface increases, hence free electrons and holes were generated and the subsequent recombination of electrons/hole with the electron/ holes trap centers gave rise to the light emission.

With the increasing impact velocity, more compression of the sample takes place, and therefore, more area of the newly created surface takes place. Thus, the ML intensity will increase with increasing value of the impact velocity. It is to be noted that the stress near the tip of a moving crack is of the order of $Y/100 \approx 10^{10}$ dynes/cm^2 = 10^9 Newton/m^2 (where Y is the Young's modulus of the materials). Thus, a fixed charge density will be produced on the newly created surfaces and the increase in the ML intensity will primarily be caused by the increase in

the rate of newly created surface area with increasing impact velocity [42]. Moreover, the total ML intensity will also increase with impact velocity because the more compression of the sample will create more surfaces with increasing impact velocity. As the impact velocity increases, the impact pressure also increases, leading to the increase in the electric field at local region which causes the decrease in trap depth. Hence the probability of de-trapping increases. From Fig. 6 (b) (inset), it can be seen that with increasing impact velocity, ML intensity also increases linearly i.e., the ML intensity of $CaZrO_3:Eu^{3+}$ (3.0%) phosphor is lineally proportional to the magnitude of the impact velocity, which suggests that this phosphor can be used as sensors to detect the stress of an object [43].

4. CONCLUSION

Orange-red emitting $CaZrO_3:xEu^{3+}$ phosphors ($1.0\% \leq x \geq 5.0\%$) were synthesized by solid state reaction. The phosphors can be effectively excited by 395 nm and exhibit orange-red emission with dominate peak at 593 nm. The optimal doping concentration is determined to be 3.0% for Eu^{3+} ions doped $CaZrO_3$ host. The life time of $CaZrO_3:Eu^{3+}$ (3.0%) phosphor can be calculated by a curve fitting technique, and the decay curves fitted by the sum of two exponential components have different decay times (τ_1 = 1.61 ms; τ_2 = 51.57 ms) and they possess the fast and slow decay process. The CIE chromaticity coordinates of $CaZrO_3:Eu^{3+}$ (3.0%) are calculated to be (x = 0.6092, y = 0.3836). The results show that the phosphor $CaZrO_3:xEu^{3+}$ could be a potential candidate for the red component of white LEDs. It is worthy to note that the dependence ML intensity to the impact velocity is close to linear, which suggests that these phosphors can be used as sensors to detect the stress of an object.

References

1. H. W. Leverenz, An Introduction to Luminescence of Solids, Dover Publications Inc., New York, (1968).

2. Z. Wang, S. Lou, P. Li, Enhanced orange–red emission of $Sr_3La(PO_4)_3:Ce^{3+}$, Mn^{2+} via energy transfer, J. Lumin. 156 (2014) 87–90.

3. J. Liu, K. Liang, Z. C. Wu, Y. M. Mei, S.P. Kuang, D. X. Li, The reduction of Eu^{3+} to Eu^{2+} in a new orange–red emission $Sr_3P_4O_{13}$:Eu phosphor prepared in air and its photoluminescence properties, Ceram Int 40 (2014) 8827–8831.

4. I. P. Sahu, D.P. Bisen, N. Brahme, R.K. Tamrakar, Studies on the luminescence behavior of $SrCaMgSi_2O_7:Eu^{3+}$phosphor by solid state reaction method, J. Electron. Mater. 27(2) (2016)1828-1839.

5. Y. Chen, X. Cheng, M. Liu, Z. Qi, C. Shi, Comparison study of the luminescent properties of the white light long afterglow phosphors: $Ca_xMgSi_2O_{5+x}:Dy^{3+}$ (x = 1, 2, 3). J Lumin 129 (2009) 531–535.

6. X. M. Zhang, F. G. Meng, C. Yang, H. J. Seo, Temperature dependence of luminescence properties of $Sr_3P_4O_{13}$: Eu^{2+} polycrystalline ceramics, J. Lumin. 140 (2013) 74–77.

7. X. G. Zhang, L. Y. Zhou, M. L. Gong, High brightness Eu^{3+} doped $Ca_3(PO_4)_2$ red phosphor for NUV light emitting diodes application, Opt. Mater. 35 (2013) 993–997.

8. R. Y. Yang, Y. M. Peng, Y. K. Su, Novel red-emitting microwave assisted sintered $LiSrPO_4$: Eu^{3+} phosphors for application in near-UV white light-emitting diodes, J. Electron. Mater. 42 (2013) 2910–2914.

9. S. Kamei, Y. Kojima, N. Nishimiya, Preparation and fluorescence properties of novel red-emitting Eu^{3+} activated amorphous alkaline earth silicate phosphors, J. Lumin. 130 (2010) 2247–2250.

10. G. Zhu, Z. Ci, Y. Shi, Y. Wang, Synthesis and photoluminescence properties of $Ca_{19}Mg_2(PO_4)_{14}:Sm^{3+}$ red phosphor for white light emitting diodes, Mater. Res. Bull. 55 (2014) 146–149.

11. P. Kumari, P. K. Baitha, J. Manam, Structural and photoluminescence properties of red-light emitting $YVO_4:Eu^{3+}$ phosphor synthesized by combustion and solid-state reaction techniques: a comparative study, Indian J Phys 89(12) (2015) 1297–1306.

12. I. P. Sahu, Enhance Luminescence by Introducing Alkali Metal Ions ($R^+ = Li^+$, Na^+ and K^+) in $SrAl_2O_4:Eu^{3+}$ Phosphor by Solid State Reaction Method, Radiat Eff. Defects Solids 171 (5–6) (2016) 511–527.

13. Z. Song, J. Liao, X. Ding, T. Zhou, Q. L. Liu, Stability of divalent/trivalent oxidation state of europium in some Sr-based inorganic compounds, J. Lumin. 132 (2012) 1768-1773.

14. C. Chang, D. Mao, Luminescent properties of $Sr_2MgSi_2O_7$ and $Ca_2MgSi_2O_7$ long lasting phosphors activated by Eu^{2+}, Dy^{3+}. J Alloy Compd 390 (2005) 133-137.

15. T. W. Kuo, T. M. Chen, Synthesis and luminescence of $Ca_4YO(BO_3)_3:Eu^{3+}$ for fluorescent lamp application. Opt. Mater. 32 (2010) 882 - 885.

16. X. Dong, J. Zhang, X. Zhang, Z. Hao, Y. Luo, New orange red phosphor $Sr_9Sc(PO_4)_7:Eu^{3+}$ for NUV-LEDs application, J. Alloys Compd. 587 (2014) 493–496.

17. S. Kamei, Y. Kojima, N. Nishimiya, Preparation and fluorescence properties of novel red-emitting Eu^{3+}-activated amorphous alkaline earth silicate, J. Lumin., 130 (2010) 2247-2250.

18. R. K. Tamrakar, D P. Bisen, K. Upadhyay, S. Tiwari, Synthesis and thermoluminescence behavior of ZrO2: Eu^{3+} with variable concentration of Eu^{3+} doped phosphor, J. Radiat. Res. Appl. Sci. 7 (4) (2014) 486-490.

19. I.P. Sahu, The role of europium and dysprosium in the bluish-green long lasting $Sr_2Al_2SiO_7:Eu^{2+}$, Dy^{3+} phosphor by solid state reaction method, J Mater Sci: Mater Electron 26(9) (2015) 7059-7072.

20. JCPDS file number 20-0254, JCPDS International Center for Diffraction Data.

21. N. Lakshminarasimhan UV Varadaraju, Luminescence and afterglow in Sr_2SiO_4: Eu^{2+}, RE^{3+} [RE= Ce, Nd, Sm and Dy] phosphors - Role of co-dopants in search for afterglow, Mater. Res. Bull. 43 (2008) 2946–2953.

22. Z. Gou, J. Chang, W. Zhai, Preparation and characiterization of novel bio-active dicalcium silicate ceramics. J Eur Ceram Soc 25 (2005) 1507–1514.

23. V. Dubey, N. Tiwari, Structural and optical analysis on europium doped AZrO3 (A=Ba, Ca, Sr) phosphor for display devices application, AIP Conference Proceedings 1728, 020002 (2016); doi: 10.1063/1.4946052.

24. G. Vicentinia, L. B. Zinner, J. Zukerman-Schpector, K. Zinner, Luminescence and structure of europium compounds, Coordination Chemistry Reviews 196 (2000) 353 – 382.

25. H. Wu, Y. Hu, Y. Wang, F. Kang, Z. Mou, Investigation on Eu^{3+} doped $Sr_2MgSi_2O_7$ red emitting phosphors for white light emitting diodes. Opt Laser Technol., 43 (2011) 1104–1110.

26. M. Mashangva, M.N. Singh, T.B. Singh, Estimation of optical trapping relevant to persistence luminescence Indian J. Pure Appl. Phys 49 (2011) 583-589.

27. J. Zheng, Q. Cheng, W. Chen, Z. Guo, C. Chen, Luminescence Properties of an Orange-Red $Ba_5(BO_3)_2(B_2O_5):Sm^{3+}$ Phosphor with High Color Purity, ECS Journal of Solid State Science and Technology, 4 (5) (2015) 72-77.

28. Z. Zhang, Y. Wu, X. Shen, Y. Ren, W. Zhang, D. Wang Enhanced novel orange red emission in $Ca_3(PO_4)_2:Sm^{3+}$ by charge compensation, Opt Laser Technol., 62 (2014) 63–68

29. J. Suresh Kumar, K. Pavani, A. Mohan Babu, N. Kumar Giri, S. B. Rai, L. R. Moorthy, Fluorescence characteristics of Dy^{3+} ions in calcium fluoroborate glasses, J. Lumin., 130 (2010) 1916-1923.

30. CIE (1931) International Commission on Illumination. Publication CIE no. 15 (E-1.3.1).

31. T. Aitasalo, J. Holsa, H. Jungner, M. Lastusaari, J. Niittykoski, Thermoluminescence Study of Persistent Luminescence Materials: Eu^{2+}- and R^{3+}-Doped Calcium Aluminates, $CaAl_2O_4:Eu^{2+}$, R^{3+}, J. Physc. Chem. B 110 (2006) 4589 - 4598.

32. K. V. D. Eeckhout , P. F. Smet, D. Poelman, Persistent Luminescence in Eu^{2+} Doped Compounds: A Review, Materials 3 (2010) 2536-2566.

33. T. Katsumata, R. Sakai, S. Komuro, T. Morikawa, "Thermally stimulated and photostimulated luminescence from long duration phosphorescent $SrAl_2O_4$:Eu,Dy crystals J. Electrochem. Soc. 150 (5) (2003) 111-114.

34. S. K Gupta, M. Kumar, V. Natarajan, S. V. Godbole, Optical properties of sol–gel derived $Sr_2SiO_4:Dy^{3+}$ Photo and thermally stimulated luminescence, Opt Mater. 35 (2013) 2320–2328.

35. M. Manam, S. Das, Determination of kinetic parameters of thermally stimulated luminescence of Cu-doped $BaSO_4$. J. Phys. Chem. Solids 70 (2009) 379–384.

36. V. Pagonis, G. Kitis, C. Furetta, Numerical and Practical Exercises in Thermoluminescence, Springer (2006).

37. I. P. Sahu, Orange-Red Emitting Europium Doped Strontium Ortho-Silicate Phosphor by Solid State Reaction Method, , J. Biol. Chem. Lumin. DOI 10.1002/bio.3188 (2016)

38. D. R. Vij. Luminescence of solids. New York: Plenum Press; **(1998).**

39. B. P. Chandra, Development of mechanoluminescence technique for impact studies, J. Lumin. 131 (2011) 1203 - 1210.

40. H. Zhang, N. Terasaki, H. Yamada, C. N. Xu, Development of mechanoluminescent micro-particles $Ca_2MgSi_2O_7$:Eu,Dy and their application in sensors, Thin Solid Films, 518 (2009) 610–613.

41. H. Zhang, N. Terasaki, H. Yamada, C. N. Xu, Blue light emission from stress activated $Sr_2MgSi_2O_7$:Eu, Int J Modern Phys B 23 (2009) 1028–1033.

42. B. P. Chandra, R. A. Rathore, Classification of mechanoluminescence, Cryst. Res. Tech. 30 (1995) 885-896.

43. H. Zhang, C. N. Xu, N. Terasaki, H. Yamada, Detection of stress distribution using $Ca_2MgSi_2O_7$:Eu, Dy microparticles, Physics E 42 (2010) 2872–2875.

Figures:-

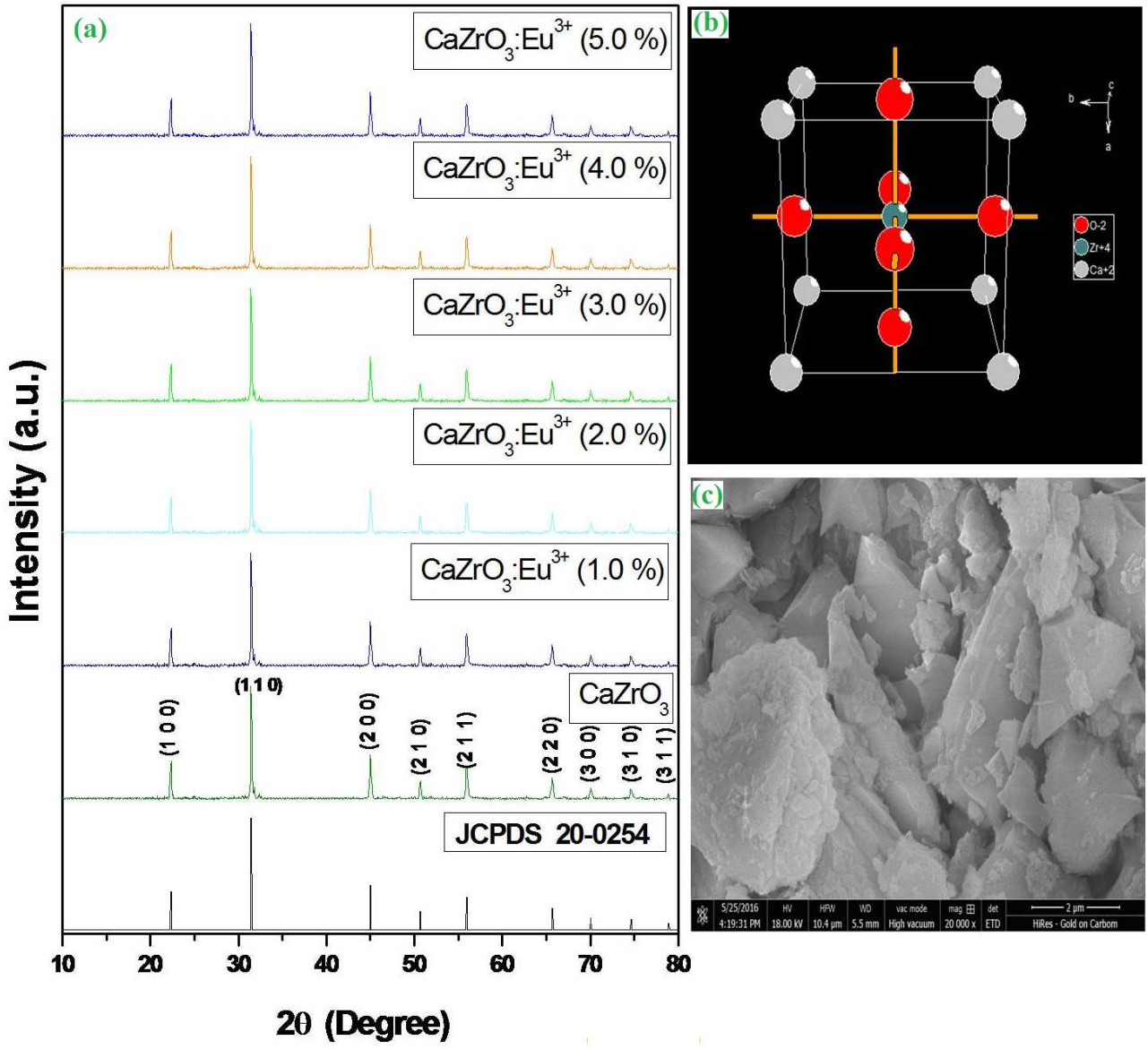

Fig. 1 (a) XRD patterns of $CaZrO_3$ and $CaZrO_3:Eu^{3+}$ phosphors with different Eu^{3+} concentration (b) Crystal structure and cation polyhedral arrangements of polymorph $CaZrO_3$ phosphor (c) FESEM image of $CaZrO_3:Eu^{3+}$ (3.0%) phosphor

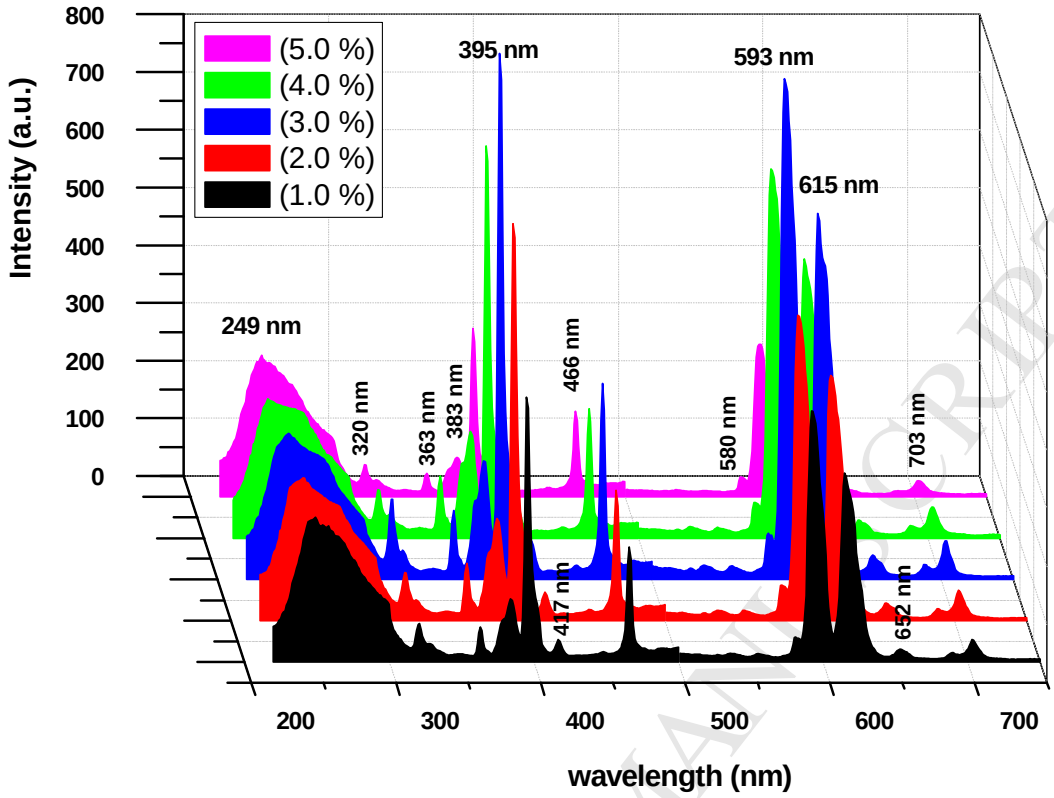

Fig. 2 Excitation and emission spectra of $CaZrO_3:xEu^{3+}$ phosphors with different Eu^{3+} concentration

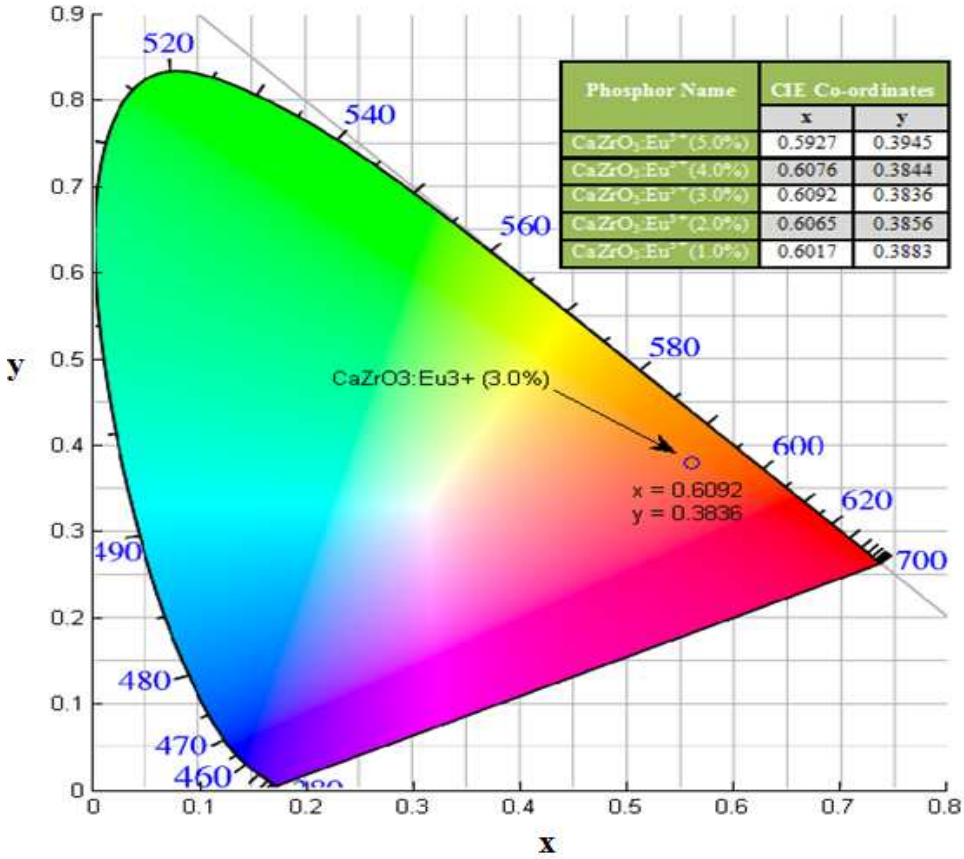

Fig. 3 CIE chromaticity diagram of $CaZrO_3:Eu^{3+}$ (3.0%) phosphor

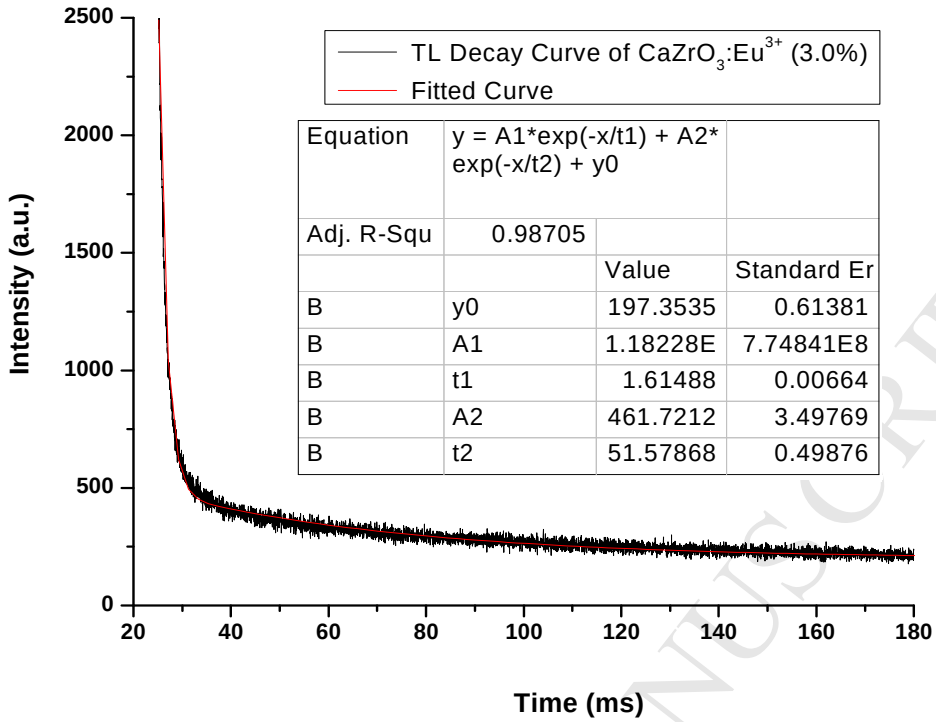

Fig. 4 Decay curves of $CaZrO_3:Eu^{3+}$ (3.0%) phosphor

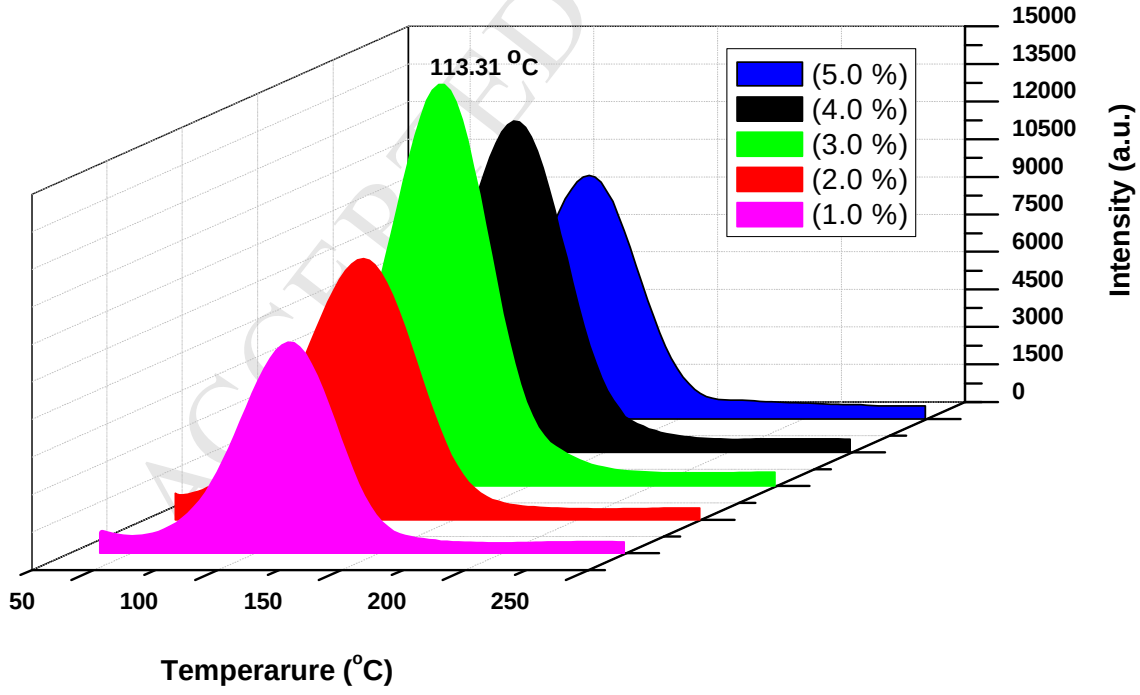

Fig. 5 (a) Comparative TL glow curve of $CaZrO_3:xEu^{3+}$ phosphors with different Eu^{3+} concentration at 5 minute UV irradiation

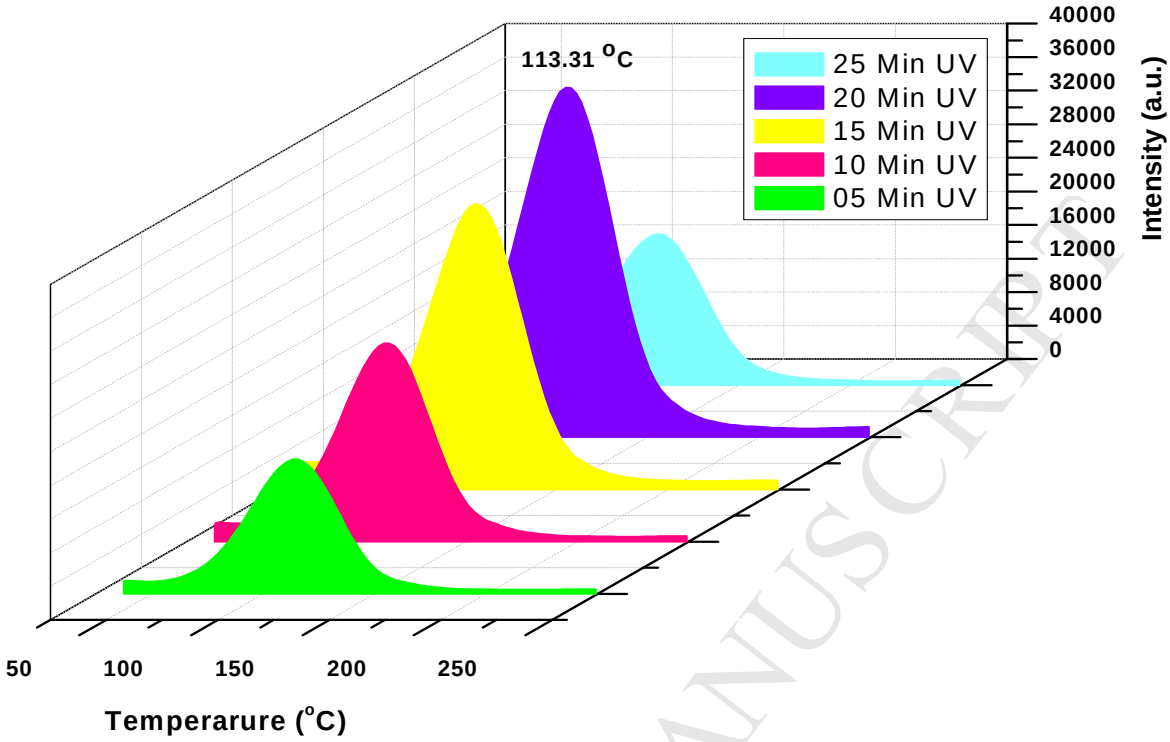

Fig. 5 (b) Comparative TL glow curve of $CaZrO_3:Eu^{3+}$ (3.0%) phosphor for different UV irradiation time

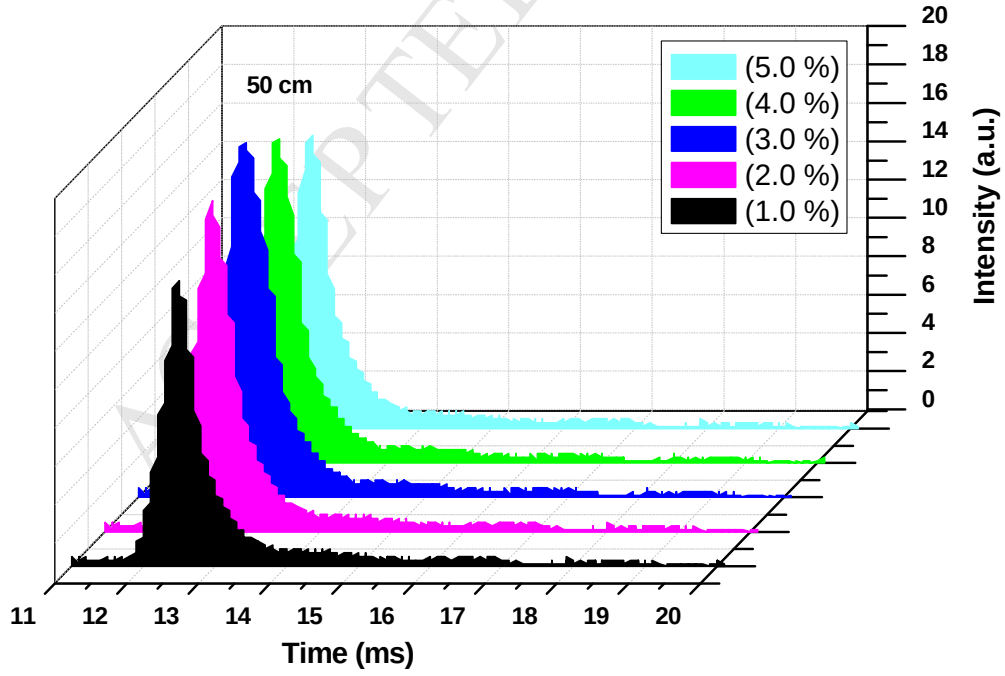

Fig. 6 (a) Comparative ML glow curve of $CaZrO_3:xEu^{3+}$ phosphors

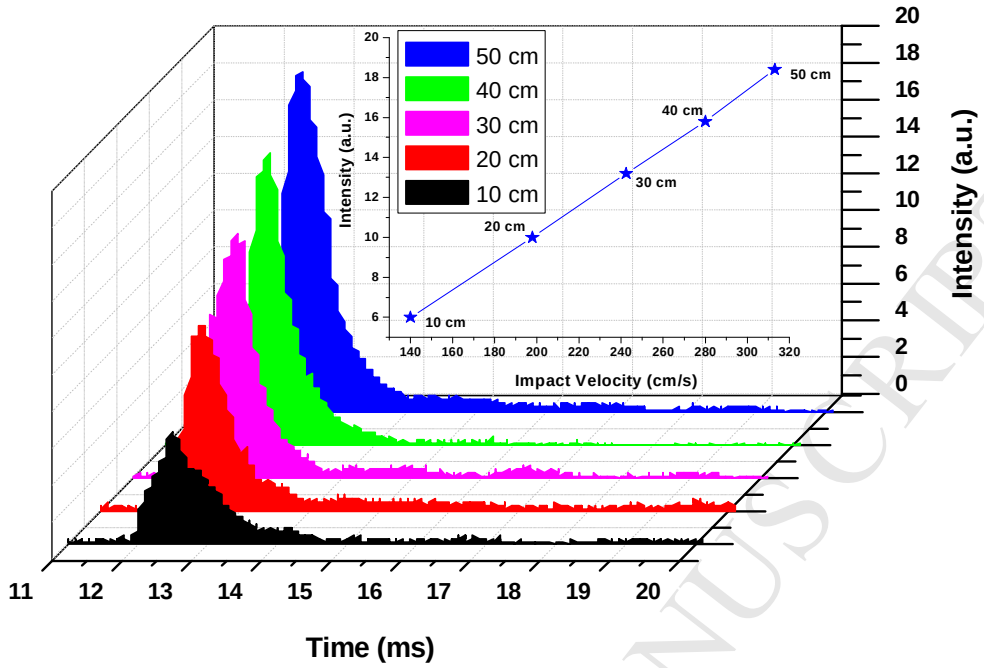

Fig. 6 (b) ML intensity versus time curve of $CaZrO_3:Eu^{3+}$ (3.0%) phosphor (Inset - ML intensity versus impact velocity curve of $CaZrO_3:Eu^{3+}$ (3.0%) phosphor)

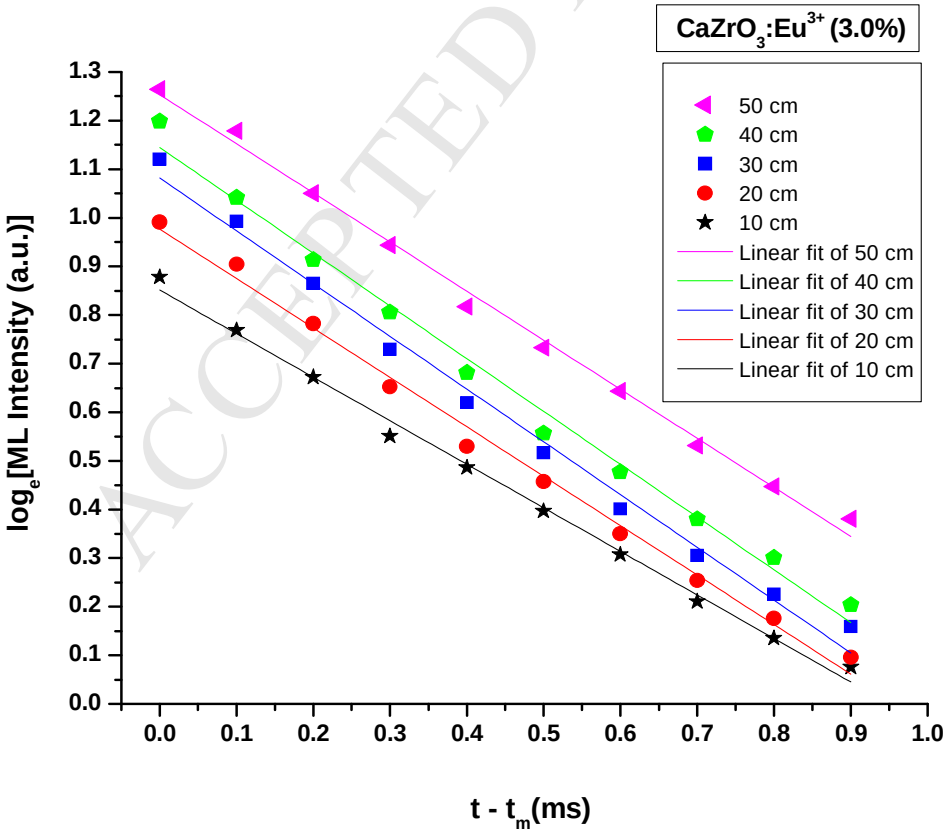

Fig. 7 Semi-log plot of ML intensity versus $(t - t_m)$ for $CaZrO_3:Eu^{3+}$ (3.0%) phosphor

Table:-

Table 1 Atomic parameters of $CaZrO_3$ phosphor

Atom	Ox.	Wyck.	Site	x/a	y/b	z/c
Ol	-2	3c	4mm.m	1/2	1/2	0
Zr1	-4	1b	m-3m	1/2	1/2	1/2
Ca1	2	1a	m-3m	0	0	0

Table 2 Activation Energy (E), Shape factor (μ_g) and Frequency Factor (s) for 5 minute UV irradiated $CaZrO_3:xEu^{3+}$ phosphors for different Eu^{3+} concentration

Phosphors Name	UV Min	HTR	T_1 (°C)	T_m (°C)	T_2 (°C)	τ (°C)	δ (°C)	ω (°C)	μ_g = δ/ω	Activation Energy (eV)	Frequency Factor
$CaZrO_3:Eu^{3+}$ (1.0%)	5	5	87.06	113.31	136.85	26.25	23.54	49.79	0.47	0.84	4.29×10^{10}
$CaZrO_3:Eu^{3+}$ (2.0%)	5	5	87.71	113.31	137.10	25.60	23.79	49.39	0.48	0.85	5.40×10^{10}
$CaZrO_3:Eu^{3+}$ (3.0%)	5	5	89.43	113.31	137.10	23.88	23.79	47.67	0.50	0.88	1.51×10^{11}
$CaZrO_3:Eu^{3+}$ (4.0%)	5	5	87.80	113.31	138.50	25.51	25.19	50.70	0.50	0.83	2.57×10^{10}
$CaZrO_3:Eu^{3+}$ (5.0%)	5	5	89.43	113.31	136.80	23.88	23.49	47.37	0.50	0.89	1.82×10^{11}

Table 3 Activation Energy (E), Shape factor (μ_g) and Frequency Factor (s) for $CaZrO_3:Eu^{3+}$ (3.0%) phosphor for different UV irradiation time

Phosphors Name	UV Min	HTR	T_1 (°C)	T_m (°C)	T_2 (°C)	τ (°C)	δ (°C)	ω (°C)	μ_g = δ/ω	Activation Energy (eV)	Frequency Factor
$CaZrO_3:Eu^{3+}$ (3.0%)	5	5	89.43	113.31	137.10	23.88	23.79	47.67	0.50	0.88	1.51×10^{11}
$CaZrO_3:Eu^{3+}$ (3.0%)	10	5	86.42	113.31	138.35	26.89	25.04	51.93	0.48	0.81	1.27×10^{11}
$CaZrO_3:Eu^{3+}$ (3.0%)	15	5	87.60	113.31	137.30	25.71	23.99	49.70	0.48	0.84	3.40×10^{10}
$CaZrO_3:Eu^{3+}$ (3.0%)	20	5	87.30	113.31	137.50	26.01	24.19	50.20	0.48	0.85	4.52×10^{10}
$CaZrO_3:Eu^{3+}$ (3.0%)	25	5	89.20	113.31	137.15	24.11	23.84	47.95	0.50	0.87	1.33×10^{10}

Table 4 Calculation of ML decay constant for $CaZrO_3:Eu^{3+}$ (3.0%) phosphor

Impact velocity	10 cm	20 cm	30 cm	40 cm	50 cm
τ Decay constant (ms)	1.11	0.98	0.92	0.92	0.99
Standard error (ms)	0.02	0.02	0.03	0.03	0.02